Journal of Ultrafine Grained and Nanostructured Materials
https://jufgnsm.ut.ac.ir
Vol. 57, No.2, December 2024, pp. 222-235
Print ISSN: 2423-6845 Online ISSN: 2423-6837
DOI: 10.22059/jufgnsm.2024.02.11

Evaluation of Mechanical Properties, Corrosion Resistance, and Microstructure of an Al 1Wt%Graphene- Al_2O_3 Hybrid Composite Sheet Produced by Accumulative Roll Bonding

Enayat Jafarzadeh[1], Laleh Ghalandari*[*,1]

[1]Department of Materials Engineering, Shiraz Branch, Islamic Azad University, Shiraz, Iran.

Recieved: 20 October 2024; Accepted: 15 December 2024

**Corresponding author email: Ghalandari@iaushiraz.ac.ir*

ABSTRACT

In the present study, the Al/Al_2O_3/Graphene hybrid metal matrix composite was processed by accumulative roll bonding (ARB). A mixture of Al_2O_3 and Graphene (0.5 Wt% for each powder) was poured between two Al layers. The process continued up to five cycles, revealing particle-free zones and clusters in the composite's microstructure. Increasing the ARB cycles improved the distribution of reinforcing particles in the aluminum matrix. Irregular porosities appeared in the early cycles and elongated in the middle ones. SEM investigation showed that better interface bonding in the last cycles increases internal stresses, promoting aluminum matrix flow and reducing porosities, crack sizes, and debonding. Mechanical tests such as tensile tests in RD directions, microhardness, fractography, and potentiodynamic corrosion tests in 3.5 wt-% NaCl solution have been performed to characterize the produced composites for the first time. Results showed that the tensile strength of the produced composites increases by increasing the ARB cycles and reaches the maximum value in the fifth cycle. Microhardness measurement indicated that the hardness of individual layers increases continuously by increasing the ARB cycles. The tensile fracture mode is a mixed fracture mode consisting of the cleavage and dimple rupture fracture in all cycles. The corrosion rate decreased from the first to the third ARB cycle relative to pure Aluminium alloy, arising from the presence of the inert particle and good bonding. However, it increased abruptly in the fifth cycle.

Keywords: *Accumulative roll bonding (ARB); Corrosion; Metal-matrix composites (MMCs); Graphene; Alumina.*

1. Introduction

The demand for highly energy-efficient structures and lightweight multifunctional composites is increasing daily. Graphene has become popular among researchers in the last decade due to its exceptional mechanical, electrical, and thermal properties. Several researchers have used graphene as a reinforcement to develop multifunctional metal matrix composites (MMCs) with the graphene-reinforced aluminum matrix composite (GAMC) attracting more attention due to its lightweight, high specific modulus, and low coefficient of thermal expansion, as well as its good wear and corrosion resistance properties. GAMC can be utilized for multidimensional applications such as lightweight structures, thermal management, and lightweight wires with high electrical conductivity[1].

Although casting and powder metallurgy are the conventional methods used to produce MMCs, they have certain drawbacks, such as high production costs and imperfections like the porosities and

accumulation of the reinforcements, leading to low homogeneity that affects the mechanical and electrical properties of the composite [2]. Moreover, additive manufacturing can be used as a reliable technique for developing graphene-reinforced MMCs. Recently, a report has been published on the successful production of GAMC with increased hardness up to ~75% using the additive manufacturing. Although these processes are remarkable for developing uniformly dispersed graphene-reinforced MMCs, the developing of a simple, cost-effective, and scalable process is crucial in meeting industrial needs [1]. To overcome these limitations, this study has focused on an alternative technique known as Accumulative Roll Bonding (ARB), which allows for the production of MMCs, while reducing the matrix grain size significantly. This technique is utilized to produce Ultra-Fine Grain (UFG) materials [2].

ARB is a process of the Severe Plastic Deformation (SPD) methods widely used to produce UFG [3–6].This method has been employed on pure metals to achieve a fine structure, to increase the material's strength, and to develop other properties [7,8]. Besides, it is also useful for producing multilayer [9] and particulate composite materials [2,10–12]. This method involves rolling and cutting the stacked sheets at each pass. Numerous researchers have attempted to produce graphene or graphene oxide-reinforced MMCs [1,10,13–17].

One of the most important and challenging issues in producing these composites is improving the layer adhesion due to the fact that graphene powders act as lubricants, thereby reducing the layer adhesion. This research aims to overcome this problem by adding the alumina powder to the graphene powder and producing an aluminum-based hybrid composite containing the graphene-alumina particles.

2. Experimental details

Fig. 1 shows the flow chart of the experimental procedure The experimental procedures first contained materials preparation, and after the composite preparation, it contained two sub-procedures: sandwich making and the ARB. After composite production, they are characterized by the method written in the flow chart, which will be described.

2.1. Materials preparation

This study has used the commercially pure 1100 aluminum of size 200×40×1 with the chemical composition listed in Table 1in Wt% as the primary sheets. The sheets were applied for the experiment

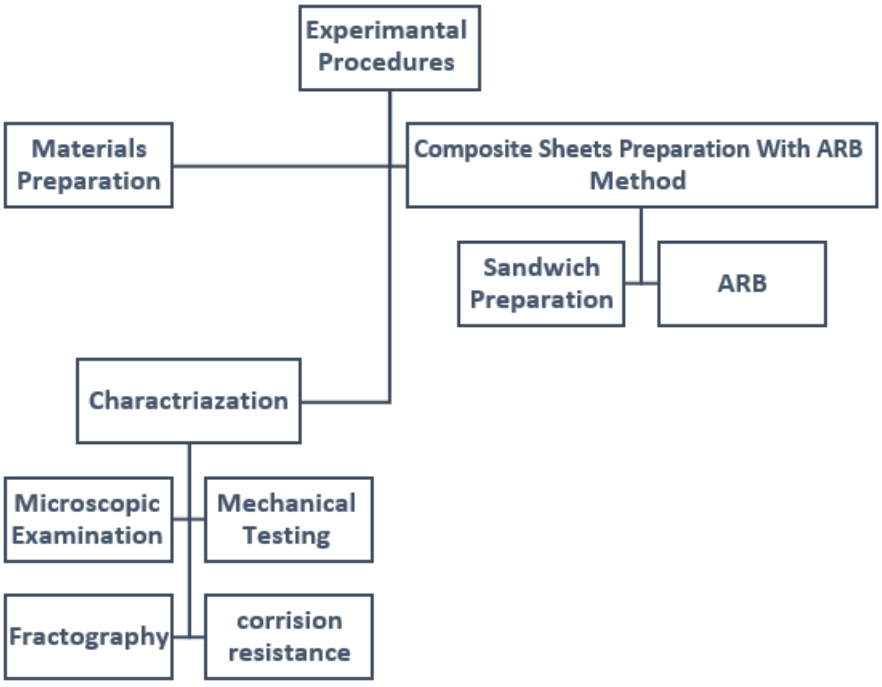

Fig. 1- Experimental procedures flow chart.

after annealing at 686°C for 2 hr. The graphene powders (Namago Co., Tehran, Iran), mixed with the alumina powder (referred to hereafter as Al_2O_3 -G), were employed as reinforcements (at a rate of around 0.5% by weight for each one).

2.2. Composite sheets preparation

The preparation of sheets consisted of two steps. At first, the surfaces were washed with acetone to remove greasy contamination and impurities. Then, the surfaces were brushed with a stainless-steel brush to remove the oxidized layer.

After that, the Al_2O_3-G particles were sieved on the sheets, and then the sheets were stacked and attached using copper wire. The stacked sheets were heated at 150 °C for 15 min in the furnace and roll-bonded immediately with a reduction of 66% in thickness, (this reduction's amount is just for the sandwich preparation cycle.), which is necessary to ensure good bonding between the neighboring Al layers.

After rolling, the obtained sheets were cut lengthwise into two equal parts, and to eliminate edge cracks and jagged edges between each pass, the edges of the samples were cut using an electric guillotine device. The process steps were repeated from the surface preparation time onward. Each process cycle is known as an ARB cycle, and in this research, the ARB process cycle was applied five times on the composite aluminum sheets. The thickness reduction in each ARB cycle was 50%. In this case, the final thickness of the sheet remained unchanged compared to the initial sheet in each cycle.

The rolling was conducted in non-lubricated conditions using a laboratory rolling mill with a roll diameter of 150 mm and a loading capacity of 20 t at a rolling speed of about 6 m/min. Fig. 2 schematically illustrates the process used to produce the composites.

Table 1- Chemical composition (wt. %) of 1100 Aluminum sheets

Al-grade	Al	Mg	Si	Fe	Cu	Mn	Zn	Cr	Ni	Ti
1100	99.344	0.0007	0.208	0.376	0.0062	0.0037	0.001	0.002	0.003	0.017

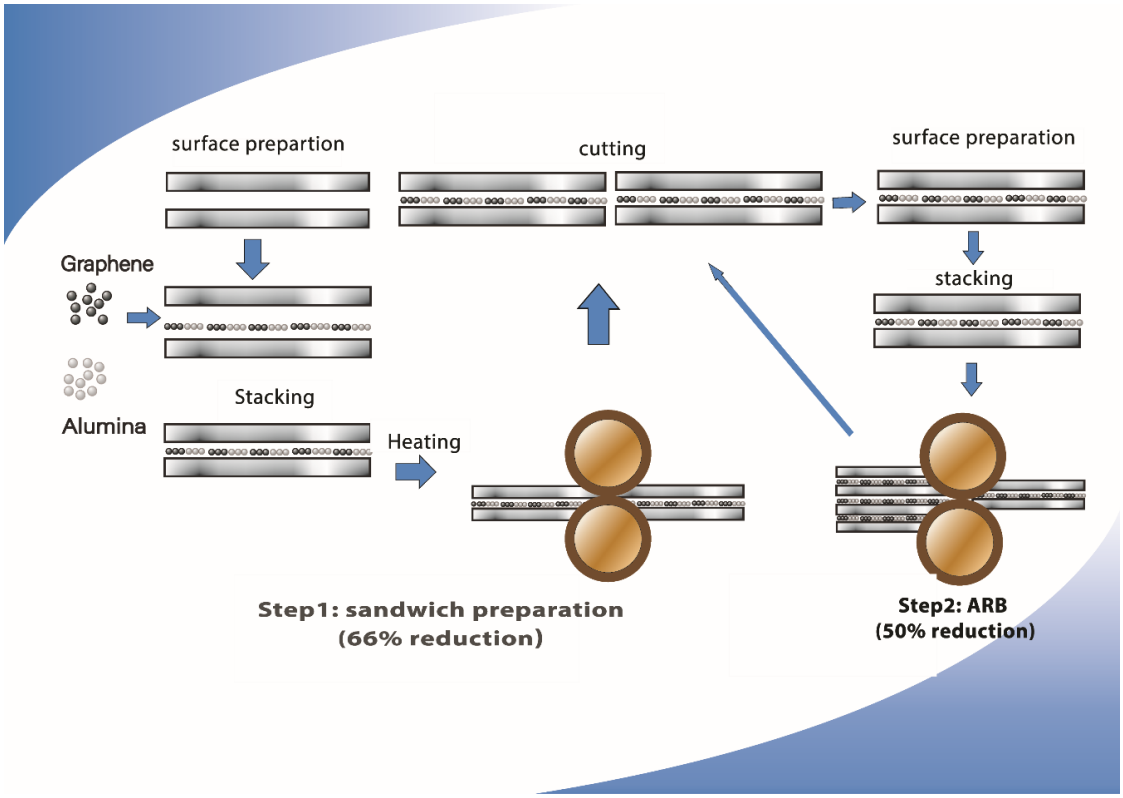

Fig. 2- Schematic illustration the ARB method.

2.3. Characterization

2.3.1. Microscopic examination

The samples were prepared, mounted in the TD-ND direction, and polished, and the microstructure of the ARB samples was finally examined. Field Emission Scanning Electron Microscope XL30HILIP (FESEM) examined the ARB samples to evaluate the bonding conditions and microstructure of the layers over different cycles.

2.3.2. Tensile and hardness test

To investigate the mechanical properties of the samples, a tensile test was performed at ambient temperature using a Hounsfield H25KS tensile machine. The tensile test samples were prepared according to the ASTM E 8M standard and in the rolling direction. After the tensile test, the engineering stress-strain curves were drawn for the ARB samples after different cycles. To measure the hardness of the samples, a Vickers indenter was utilized with the force of 10 gr for the duration of 20 s, and the microhardness was measured along the thickness of the samples.

2.3.3. Examining the fracture surface

The FESEM scanning electron microscope was used to examine the bonding between different layers and the type of surface fracture after tensile testing.

3. Results and discussion

Fig. 3 reveals the electron microscope images of the produced hybrid-composite microstructure during the different cycles of the ARB process. Due to the low magnification, the individual reinforcing particles are not visible. However, in some images such as in Figs. 3b,d, and f the agglomeration of the reinforcing particles in the layered composite structure can be observed. This agglomeration can originate from the composite production method of the composite (the ARB method). The reinforcing particles are sprinkled between the layers, creating a composite in which some regions contain agglomerated particles, while some others are free from particles (PFZ). By increasing the ARB cycles the number of layers increases and their thickness decreases so that the distribution of reinforcement particles within the aluminum matrix can gradually be improved. Besides, the Figure shows that from the first to the fifth ARB cycle, there exists a marked improvement in the bonding of the aluminum layers owing to the rising imposed strain caused by rolling deformation.

The improvement of the layers bonding by increasing the ARB cycles can be explained via the film theory [18] when two clean and brushed aluminum surfaces are placed one on the other and rolled. During the rolling process the oxide layer on the aluminum layer breaks and, subsequently, the materials of the bottom and upper layers extrude from the created cracks, reach each other, and weld together.

In this research, the agglomerated hybrid reinforcing particles have emerged from the grooves and extended in the rolling direction, changing their type from dense clusters to diffuse ones [19]. Hence, the fresh matrix exists between the particles and welds to the matrix from the other layers. Apart from this, cracks and debonding have been observed in the interlayer zone microstructure of all cycles as well. However, the thickness of the hybrid particulate-containing layers interfaces is reduced and separated in certain regions. The rolling process comprises two types of stresses. One is shear stresses, which are caused by the contact between the sheet's surface and that of the sheets and rollers. The second one is compressive stresses, which constitute horizontal and vertical components. These stresses lead to the aluminum matrix flow in all directions, accounting for the loss of porosities and lowering the crack size and debonding in the interlayer zones.

Fig. 4 shows the SEM image, the qualitative elemental microanalysis of the aluminum matrix composite with alumina and graphene reinforcing particles during the first cycle of the ARB process (under high magnification). Based upon the qualitative EDS elemental analysis, the white particles could be related to alumina particles, and the black particles pertain to graphene particles. According to the energy-dispersive spectroscopy (EDS) results, the presence of oxygen, carbon, and aluminum at Point B, as well as aluminum and carbon at Point A, has been verified. Fig. 5 shows the SEM images related to the first, the second, and the fifth cycle with relatively high magnification. The images reveal that alumina and graphene particles are clustered together in certain areas of the composite structure, while some regions are free of reinforcing particles. These particle-free zones (PFZ), indicated by yellow ovals, are far from the layer boundaries in the initial stages, yet at the fifth stage, due to the reduction of layer thickness and the proximity of the boundaries, they are alsovisible near the boundaries.

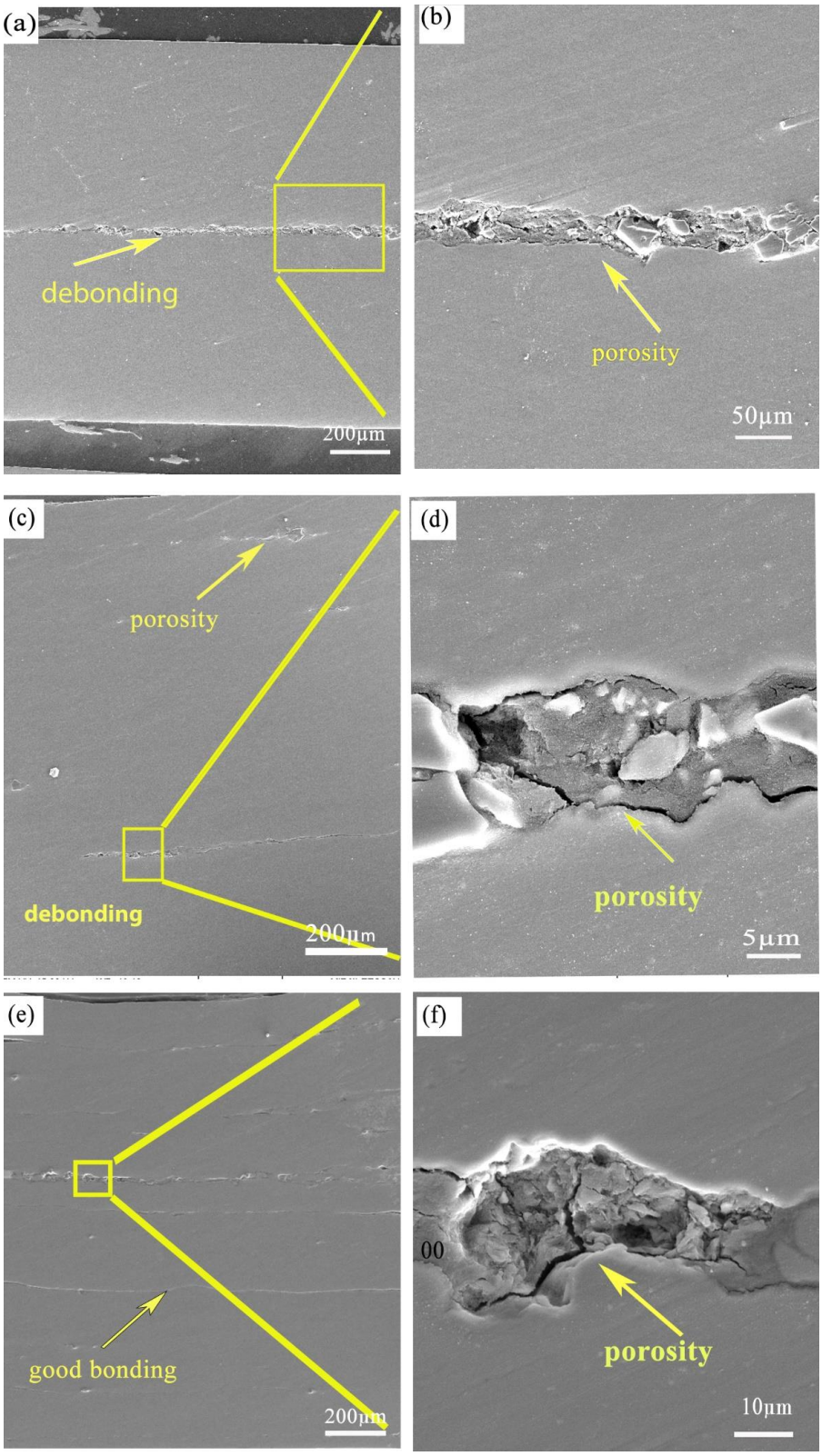

Fig. 3- (a) SEM micrographs of ARB-processed hybrid composites after (a, b) Cycle 1, (c,d) Cycle 3, and (e,f) Cycle 5 with different magnifications.

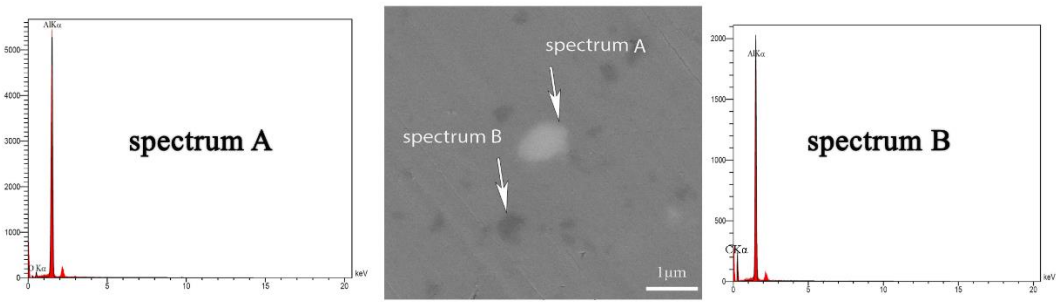

Quantitative Results for specrum A

Elt	Line	Int	Error	K	Kr	W%	A%	ZAF	Formula	Ox%	Cat#
C	Ka	38.6	3.1501	0.1388	0.0694	50.06	69.12	0.1387		0.00	0.00
O	Ka	0.9	3.1501	0.0017	0.0008	0.44	0.46	0.1911		0.00	0.00
Al	Ka	1371.2	20.1775	0.8596	0.4301	49.50	30.43	0.8688		0.00	0.00
				1.0000	0.5004	100.00	100.00			0.00	0.00

Quantitative Results for specrum B

Elt	Line	Int	Error	K	Kr	W%	A%	ZAF	Formula	Ox%	Cat#
C	Ka	78.2	33.4677	0.2516	0.1088	61.66	78.32	0.1764		0.00	0.00
Al	Ka	1332.9	36.2337	0.7484	0.3236	38.34	21.68	0.8440		0.00	0.00
				1.0000	0.4324	100.00	100.00			0.00	0.00

Fig. 4- (a) A typical SEM image of the hybrid composite after the first cycle used to identify the particles, and (b) and (c) EDS results corresponding to points A and B, respectively.

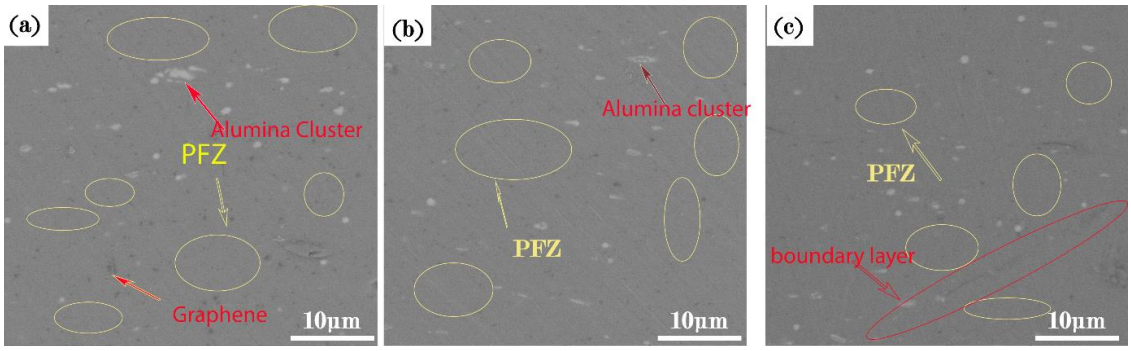

Fig. 5- SEM micrograph of the composite within the RD–TD plane after a) the first, b) the second, and c) the fifth ARB cycle, showing PFZ zones and the clusters of the particles.

Fig. 6 shows the SEM images of the produced hybrid composites related to the third cycle of the ARB process with different magnifications. In Fig. 6a, it seems that the layer bonding at this stage of the ARB process is weak. Nevertheless, the higher magnifications (Figs. 6b & 6c) reveal that the dark areas can be related to the particles. The visibility of the aluminum matrix between the particles in the interlayer zone is noticeable and shows the gradual mixing of the background and particles. Another critical point in the image is to do with the porosities. They can be observed further in the clusters of the reinforcing particles, as well as between the aluminum matrix and the reinforcing particles, as shown in Fig. 6c. Porosities in the matrix can act as suitable sites for crack nucleation.

3.1. Mechanical properties

Figs. 7a and 7b present the engineering stress-strain curves of the produced hybrid composite

and pure Aluminum in different ARB cycles, respectively. The tensile strength of the produced composites increased by increasing the ARB cycles and reached the maximum value in the fifth cycle. Comparing Figs. 7a and 7b revealed 2.2 times increases in the ultimate tensile strength of the ARB-processed composite in the fifth cycle, as compared with the annealed pure aluminum sample.

Fig.8 reveals the data on the amount of tensile strength and percent elongation of the produced composites from the first to the fifth cycles. As can be seen, from the first to the third cycle there was a moderate growth in the tensile strength. From the third to the fifth cycle, this number almost leveled off.

In the particulate composites produced by the ARB method, two groups of factors affect the decreasing and increasing strength of the composites. The factors increasing the strength are as follows: One is the strain hardening in the initial cycles and grain refining in the last cycles [20].

Strain hardening results from the increased dislocation density within the grains or the formation of low-angle dislocation boundaries. In the final stages, the dislocation boundaries misorientation increases, and the high-angle grain boundary areas grow. As a result, the grain refinement and ultra-fine structure formation will increase the strength [1]. Another one is the particles (Al_2O_3 and graphene in this case) which obstruct the dislocation motion, leading to the dislocation accumulation and the strengthening of the composites [21]. Overall, the second-phase particles influence both the density and the distribution of dislocations. Strengthening due to the dispersion of particles depends upon the deformability and the particle strength.

When a particle deforms, its size on the slip plane is reduced effectively due to the Burgers vector 'b' of the dislocation. A smaller particle tends to be weaker than a larger particle, which softens the slip plane. This results in the subsequent dislocations moving on the same plane, concentrating the slip into bands, and increasing the heterogeneity of the deformation. In contrast, in the case of the non-deformable particles, the dislocation debris left by the previous dislocations (e.g., the Orowan loops) makes it more difficult for the slip to occur on the same plane, which tends to make the slip relatively homogeneous [22].

Should a deforming matrix contain non-deformable particles, there will be a strain incompatibility between the two phases. This incongruous state can be accommodated by generating dislocations at the particle-matrix interface, termed the Geometrically Necessary Dislocations (GNDs) around the particles, and should the interface be weak, it could be accommodated by forming voids [23]. The created Orowan loops and GNDs increase the dislocation density. Besides, the created loops decrease the mean particle spacing effectively and increase the stress required to move the subsequent dislocations. Accordingly, particle-reinforced composites have higher strain hardening rates than monolithic materials [18].

The significant increase in dislocation density alloys containing small non-deformable particles is solely obtained for minor strains. At the higher strains, the dynamic recovery may reduce the dislocation density to a value which is a little more than that pertinent to a single-phase alloy [23]. Besides, increasing the ARB cycles leads to a more homogeneous particle distribution and a decreased particle distance, thereby increasing the tensile

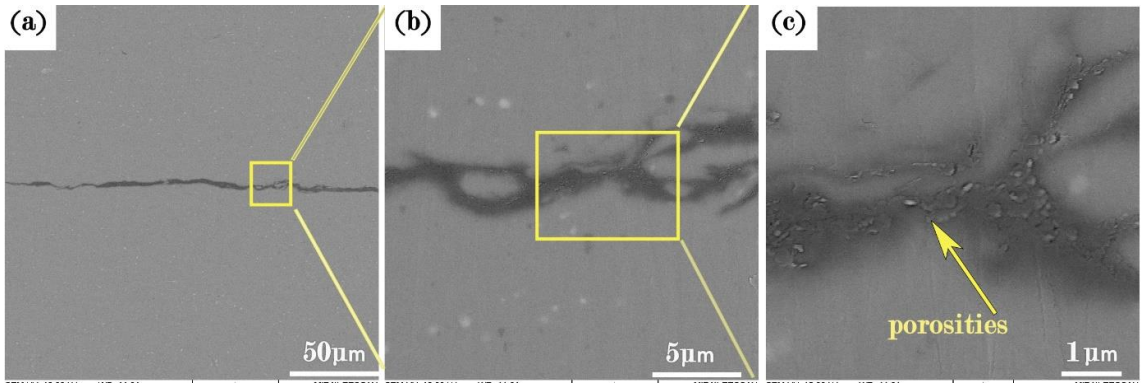

Fig. 6- SEM micrograph of the composite within the RD–TD plane after the third ARB cycle with different magnifications

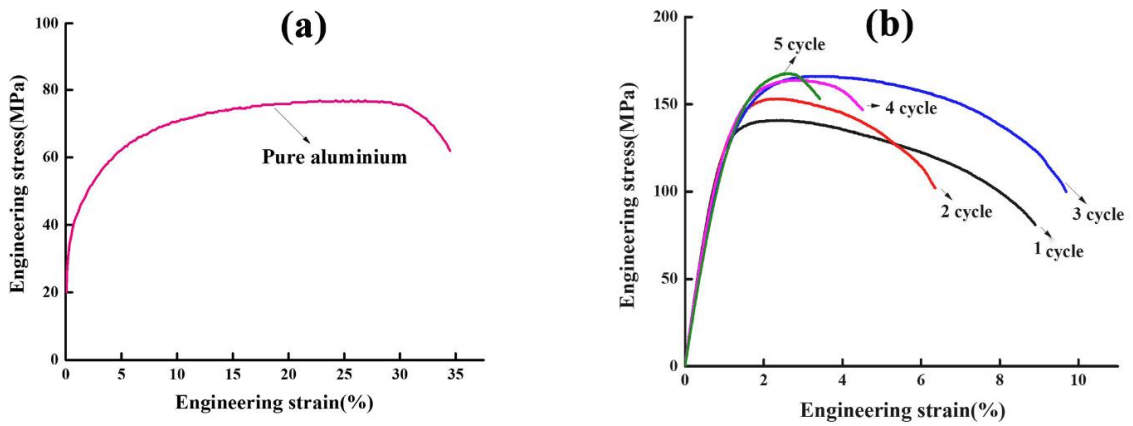

Fig. 7- Engineering stress-strain curves of the a): annealed aluminum and b): ARB-processed composite samples.

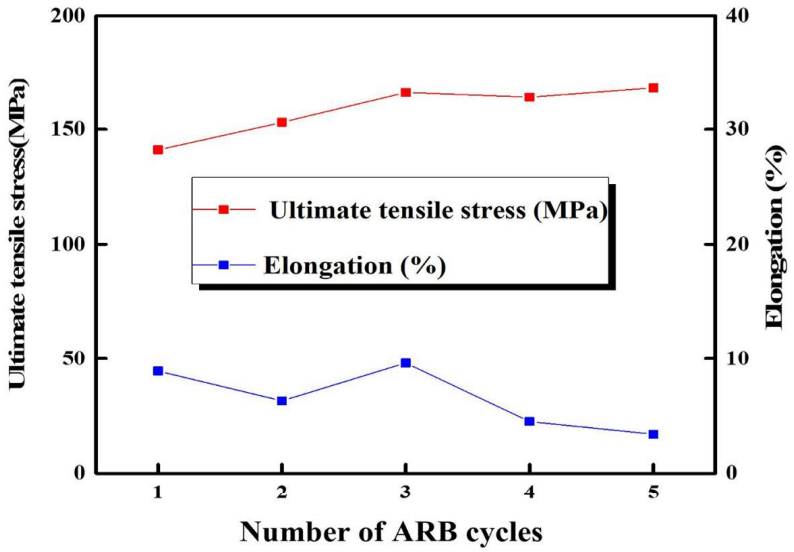

Fig. 8- Engineering stress-strain curves of the a): annealed aluminum and b): ARB-processed composite samples.

strength [24]. Also, by increasing the number of cycles and the amount of rolling pressure the clusters of the reinforcing particles separate from each other and the number of porosities decreases, leading to a rise in the composites strength. These results are consistent with other researchers' findings [21,25].

The factors leading to a reduction in strength are the weak bonding of the layer, the porosities, and cracks existing in the particle clusters, matrix, and reinforcement interfaces, and the dynamic recovery and recrystallization processes [26].

The factors leading to an increase or a decrease, which have been discussed above, contribute to the tensile strength variation of the produced composites. In the final stages of the ARB process, the tensile strength of the produced composites remains almost constant. Due to the cracks and voids in the layers and particulate interfaces (Figs. 3 and 6) and the activation of dynamic recovery, the strength of the produced composites has risen slightly.

The data on the percent elongation of the composites produced over the five ARB cycles has also been presented in Fig. 8. As can be seen, this value decreased remarkedly from about 35% for the annealed aluminum to around 5% after the first cycle. This reduction can result from the increasing dislocation density and weak bonding in certain interlayer regions. The same trend can be observed

in many other researches using the ARB process to produce composite materials [9,18,27]. From the first to the last ARB cycle, there are usually overall downward and upward trends in the percent elongation and tensile strength, respectively. As the applied strain increases, the material's strength also rises, yet eventually reaches a saturation point. However, the material's ductility decreases significantly with only a relatively small increase in strain, and then either remains constant or declines slightly as the strain continues to rise. This behavior can be observed by the percent elongation in the initial stages of each SPD process [28].

A decrease in the percent elongation of the SPD- or ARB-processed samples is due to a significant increase in dislocation density and the accumulation of internal stresses. These factors promote the nucleation of cracks, which results in a sharp drop in the percent elongation. On the other hand, a slight increase in the percent elongation with the rising ARB cycle is attributed to the bonding strength increase of the layers. When the interface bonding improves, the elongation can be increased by delaying the formation of cracks at the layer interface and the particle-matrix interface. The elongation is also increased when the distribution of the particles in the hybrid composite becomes uniform, resulting from a reduction in the probability of creating cracks at the particle sites [25].

Fig. 9 presents data on the amount of Vickers hardness value during the five ARB cycles. The hardness value gradually increased from 39 to 57 HV from the first to the fifth cycle. The Vickers microhardness of pure annealed aluminum 1100 is 31.5HV. After the first ARB cycle, the hardness increases to 1.24 times that of pure aluminum, reaching 1.8 times by the fifth cycle. Strain hardening and reinforced particles are the reason for an increase in hardness in the first ARB cycles. In the middle and high cycles, the strain hardening phenomenon does not work like in the first cycles. This can result from activating the dynamic recovery or recrystallization (the softening mechanism).

The hardness value resembles the UTS value regarding the gradual upward trend by increasing the number of ARB cycles. The mechanisms attributed to the hardness variations are similar to those discussed for UTS. However, the hardness of the ARB-processed materials is affected by a few other factors, such as the oxide layer at interfaces, the depth of the removed material during surface preparation, and the load/indentation depth; the number of indents can be applied on the particle-free zones showing low hardness values; and some indents can be applied on the particle clusters, depicting high hardness values [18].

The Vickers hardness of the produced hybrid composites increased until the fifth cycle. Unlike some of the earlier researches, it did not remain steady in the middle cycles, originating from the presence of alumina and graphene particles. In the last cycles, the distance between the particles decreased, leading to further indents on the particle clusters, which have higher hardness values than the aluminum matrix [18].

3.2. Fractography

Fig. 10 reveals the fracture surfaces of the produced hybrid composites after different ARB cycles with different magnifications related to the first, the third, and the fifth cycle, respectively.

The important features that can be concluded from the figure are the fracture modes, delamination of the layers; and particles on the fracture surfaces.

As can be seen, the fracture mechanism in all three cycles are the mixed fracture mode consisting of the cleavage and dimple rupture fracture in this cycle. The ductile fracture with the dimple rupture mode consists of void nucleation, growth, and coalescence. The microvoids nucleate in the places with the localized strain discontinuity, such as the second-phase particles, inclusions, grain boundaries, and dislocation pile-ups. As the strain in the material continues to build up, the microvoids grow and merge until they create a

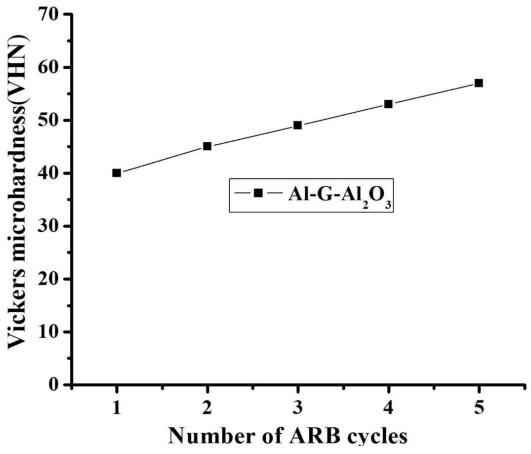

Fig. 9- Engineering stress-strain curves of the a): annealed aluminum and b): ARB-processed composite samples.

continuous fracture surface. This type of fracture, called dimple rupture, produces many small cup-shaped dimples resulting from the merging of voids [29].

Another feature of the ductile part of the fracture surface is the elongated dimples. One axis is longer than the others, and one end is open in these dimples. As a result of the shear loading condition, they are not thoroughly surrounded by a rim. [30].

Fig. 10e, related to the third cycle, reveals the chevron pattern (the sign of the brittle fracture) and dimples, showing a mixed fracture mode. In the fifth cycle the fraction of river patterns relative to the dimples increased (Fig. 10f), which correlates with the fact that by increasing the number of ARB cycles, the ductility of the material is reduced, arising from strain hardening. This is in agreement with the previous researchers' findings [31]. Various dimple sizes can be observed in the surface fractures of the produced composites, blue ovals in Fig. 10d, resulting from the nonuniform distribution of nucleating particles and the nucleation and growth of the isolated microvoids early in the loading cycle producing a fracture surface that exhibits various dimples.

After the first cycle, there were two layers and one interface. After the fifth cycle, these numbers increased to 32 and 31. Among 31 interfaces, 16 interfaces had hybrid particle clusters, which are more suitable places for crack and microvoid nucleation during the tensile or shear force exertion, and 15 are appropriate for this purpose, yet with a lower degree. As shown in Figs. 10a and 10f, the interfaces are visible, especially the last ones indicated by the arrows. As the rolling pressure increases, the strength of the two types of interface increases, and the delamination becomes slighter [4,19,21,26].

3.3. Corrosion resistance

Fig. 11 displays the potentiodynamic polarization curves of the pure annealed 1100 Al and hybrid composites after the different ARB cycles, namely the first, the third, and the fifth cycle, respectively, in a 3.5 wt.% NaCl solution. All of the curves have similar shapes, showing smooth and linear changes in the current around the rest potential, indicating the cathodic and anodic Tafel behavior [32].

The graphs in Figs. 12a and b present the calculated parameters (namely, the corrosion potential, and corrosion current) obtained from the polarization diagrams. As shown in Fig. 12a, all samples exhibit active behavior in the anodic potential, indicating the formation of a non-

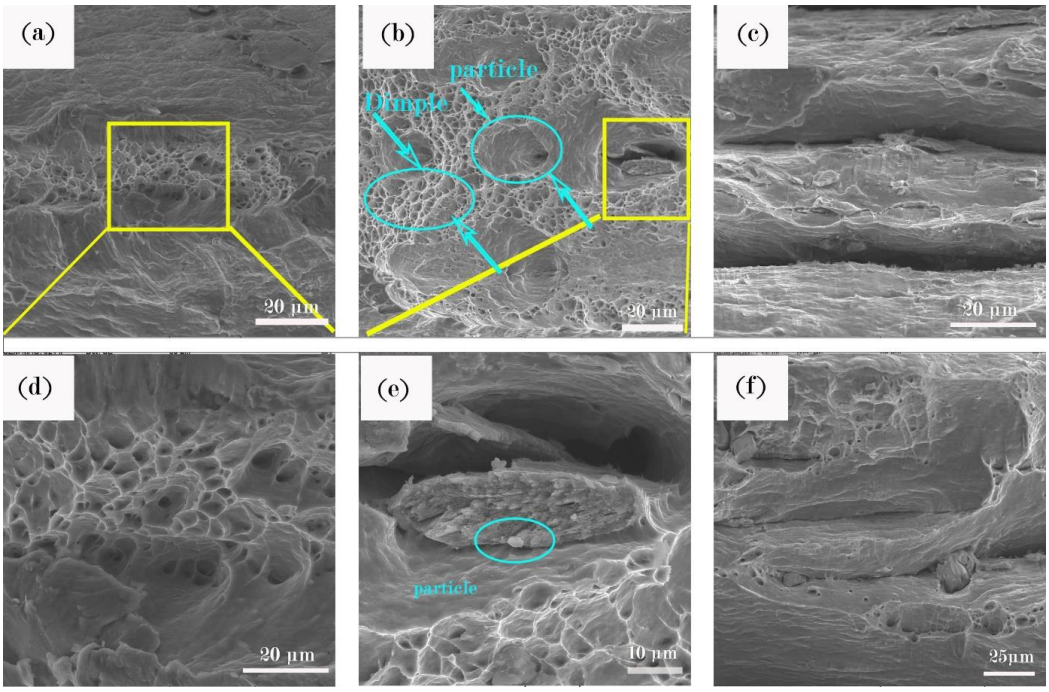

Fig. 10- The tensile fracture surface of (a) and (d) the first cycle: low and high magnification; (b) and (e) the Third cycle with low and high magnification; (c) and (f) the fifth cycle.

protective passive film. The corrosion potentials (Ecorr) of the produced hybrid composites and pure aluminum are negative and are in the same range, indicating they are thermodynamically active. The increased energy state and the active sites in the ARB-processed hybrid composites shift the corrosion potential to more negative values, reiterating the key points of our research on corrosion behavior in hybrid composites. A passive alumina film typically covers the aluminum surface and its alloys due to the chemical reaction with air. However, aluminum and its alloys are susceptible to pitting corrosion in the aqueous media, which can hinder the formation of the protective passive film [33].

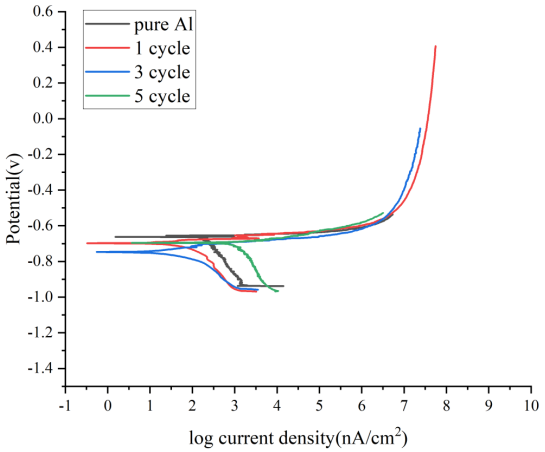

Fig. 11- potentiodynamic polarization curves of pure Aluminum and produced hybrid composites at different ARB passes.

Overall, the applied processing technique influences the samples' corrosion. The corrosion potential, E corr, represents a thermodynamic characteristic of a given metal–electrolyte system rather than the kinetics of material corrosion. In contrast, the corrosion current density, Icorr, reflects the corrosion rate more accurately.

Fig. 12b presents data on the corrosion current density (Icorr.) amount. As can be seen, the maximum Icorr. , which is 867 nA/cm^2 „ belong to the produced hybrid composite after the fifth cycle, whereas the minimum one, which is 18.5 nA/cm^2, relevant to the third cycle. The second greatest amount, which is 192 nA/cm^2, pertain to pure annealed Al. Hence, there is a one-tenth decrease in the corrosion current density of the produced hybrid composite after the third cycle with respect to the annealed pure aluminum. These amounts have abruptly increased in the fifth cycle. As can be seen, the corrosion resistance of the produced composites is higher than that of the pure annealed aluminum except for the samples pertinent to the fifth cycle.

The pitting corrosion of Al and its alloys in a halide-containing solution involves four stages: the adsorption of Cl-by oxide film, the oxide layer breakdown and penetration of aggressive ions into it, the formation of metastable pits, and the stable pit growth [34].

The produced hybrid composite microstructure has three different features in comparison to pure aluminum, which has led to notable differences in its corrosion properties.

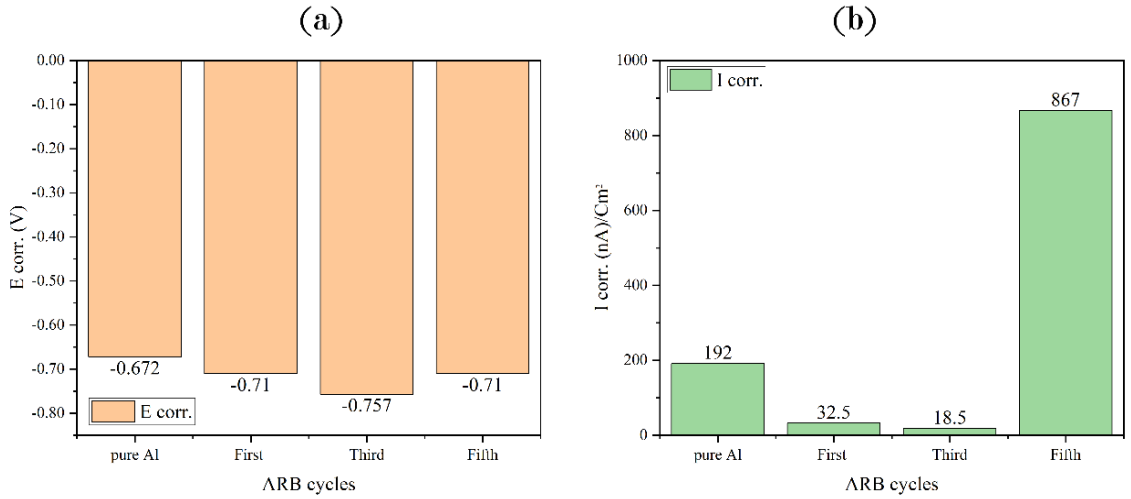

Fig. 12- (a) Variation of corrosion potentials, (b) and corrosion current density vs. ARB cycles.

The presence of graphene and alumina inert particles can hinder the penetration of aggressive ions into it and the formation of metastable pits. Thus, they can delay the formation of metastable pits. Besides, a particle acts as a relative barrier to the initiation and development of corrosion pits [35]. Inert particles cause a decrease in the activity of the surface and the cathodic reaction rate [33].

Implementing the accumulative roll bonding method on the hybrid composite has increased the density of the dislocation, the boundaries, and the other defects, thereby decreasing the corrosion resistance of the composites produced [36]. The oxide film that forms on such a high-energy and defective substrate seems to be more defective and more susceptible to pitting corrosion.

The presence of the ceramic particles in the layers' boundaries accounts for the weak layer bounding in some regions, especially around the particles. The nature of the interfacial bond, whether weak or strong, is critical in the corrosion process.

The decrease in the corrosion rate from the first to the third ARB cycle relative to pure Aluminium alloy can result from the presence of the inert particle and good bonding, and the abrupt corrosion rate increase in the fifth cycle can originate from increasing defects density and weak bonding. In the fifth cycle, the number of layers and interfaces increases; thus, the probability of weak bonding increases.

Fig. 13 depicts the morphologies of the corroded surfaces via the optical microscopy of the above samples. The pits are being observed on the samples surfaces in all four images. These results confirm the above claim about the reason for the active behavior of all the samples.

4. Conclusion

- The Al/Al_2O_3/graphene hybrid composite was produced successfully in the form of a sheet through the ARB process. A uniform distribution of the particles was not observed in the microstructure. However, by increasing the ARB cycles the number of layers increased, and their thickness decreased so that the distribution of the reinforcing particles within the aluminum matrix could improve gradually as the particles had been sprinkled between the layers.

- Several irregular porosities were observed in the low ARB cycles and elongated in the middle cycles. From the SEM investigations, it was concluded that the bonding at interfaces improves the existing stresses and leads to the aluminum matrix flow in all directions, accounting for the loss of porosities and the lowering of the crack size and the debonding in the interlayer zones.

- In view of the existing factors leading to an increase and a decrease in strength, from the first to the third cycle there was a moderate growth in the

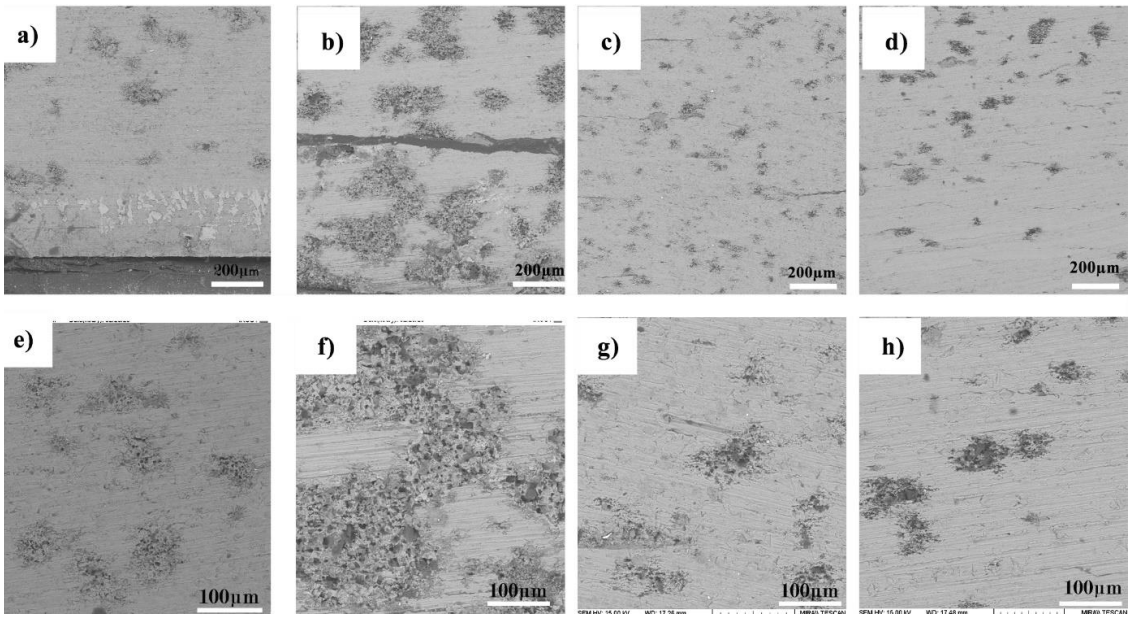

Fig. 13- optical micrographs of the corroded surface of: (a,e)pure Aluminum, (b,f)the first cycle. (c,e) the third cycle and, (d,h) the fifth cycle.

tensile strength, and from the third to the fifth cycle this amount grew gradually. Overall, the amounts of measured strengths in the entire cycles were greater than those related to the monolithic Al.

- As a result of increasing the dislocation density and weak bonding in certain interlayer regions, the percent elongation value of the produced composites was diminished remarkedly from about 35% for annealed aluminum to around 5% after the first cycle and decreased slightly until the last cycle.

- The Vickers hardness of the produced hybrid composites increased until the fifth cycle, resulting from the presence of alumina and graphene particles after the initial ARB cycles. The percent elongation dropped remarkably due to the considerable quantity of strain hardening.

- fracture mechanisms were mixed fracture mode consisting of the cleavage and dimple rupture fracture in all cycles. The brittle fracture area increased compared to the ductile fracture area as a result of strain hardening.

- The corrosion rate decreased from the first to the third ARB cycle relative to pure Aluminium alloy, arising from the presence of the inert particle and good bonding. After that, it increased abruptly in the fifth cycle, originating from increasing defect density and weak bonding. The pits were observed on the optical microscopic pictures of the corroded surfaces of all samples; this confirms their active behavior.

Acknowledgment

we are grateful to Dr. Mohammad Mehdi Mahdavian for his assistance with data collection and analysis.

Declarations

Conflict of interest: L. Ghalandari and E. Jafarzadeh declare no conflict of interest.

References

1. Tiwari JK, Mandal A, Rudra A, et al. Evaluation of mechanical and thermal properties of bilayer graphene reinforced aluminum matrix composite produced by hot accumulative roll bonding. Journal of Alloys and Compounds 2019;801:49–59.
2. Ferreira F, Ferreira I, Camacho E, et al. Graphene oxide-reinforced aluminium-matrix nanostructured composites fabricated by accumulative roll bonding. Composites Part B: Engineering 2019;164:265–271.
3. Volokitin A, Kuzmin S. Obtaining long products by severe plastic deformation methods: A Review. Journal of Ultrafine Grained and Nanostructured Materials 2023;56:84–98.
4. Sarkari Khorrami M. Friction stir welding of ultrafine grained aluminum alloys: a review. Journal of Ultrafine Grained and Nanostructured Materials 2021;54:1–20.
5. Mirzadeh H. Superplasticity of fine-grained austenitic stainless steels: A review. Journal of Ultrafine Grained and Nanostructured Materials 2023;56:27–41.
6. Esbolat A, Panin E, Arbuz A, et al. Development of Asymmetric Rolling as a Severe Plastic Deformation Method: A Review. Journal of Ultrafine Grained and Nanostructured Materials 2022;55:97–111.
7. Hosseini SA, Manesh HD. High-strength, high-conductivity ultra-fine grains commercial pure copper produced by ARB process. Materials and Design 2009;30:2911–2918.
8. Ebrahimi M, Wang Q. Accumulative roll-bonding of aluminum alloys and composites: An overview of properties and performance. Journal of Materials Research and Technology 2022;19:4381–4403.
9. Mahmoud Esmaeil Zadeh LG· RS· EJ. Microstructural Evaluation, Mechanical Properties, and Corrosion Behavior of the Al/Cu/Brass Multilayered Composite Produced by the ARB Process. Metals and Materials International 2023.
10. Ghazanlou SI, Eghbali B, Petrov R. Microstructural evolution and strengthening mechanisms in Al7075/ graphene nano-plates/ carbon nano-tubes composite processed through accumulative roll bonding. Materials Science and Engineering: A 2021;807.
11. Melaibari A, Fathy A, Mansouri M, et al. Experimental and numerical investigation on strengthening mechanisms of nanostructured Al-SiC composites. Journal of Alloys and Compounds 2019;774:1123–1132.
12. Yang XY, Mei QS, Mei XM, et al. Materials Science & Engineering A Al matrix composites reinforced by high volume fraction of TiAl 3 fabricated through combined accumulative roll-bonding processes 2019;754:309–317.
13. Omran HN, Eivani AR, Farbakhti M, et al. Tribological properties of copper-graphene (CuG) composite fabricated by accumulative roll bonding. Journal of Materials Research and Technology 2023;25:4650–4657.
14. Ferreira FB. Microstructural and Mechanical Characterization of Graphene Oxide-Reinforced Aluminium-Matrix Nanostructured Composites fabricated by Accumulative Roll Bonding 2017.
15. Fattahi M, Rostami M, Amirkhanlu F, et al. Fabrication of aluminum TIG welding filler rods reinforced by ZrO2/reduced graphene oxide hybrid nanoparticles via accumulative roll bonding. Diamond and Related Materials 2019;99:107518.
16. Liu X, Wei D, Zhuang L, et al. Fabrication of high-strength graphene nanosheets/Cu composites by accumulative roll bonding. Materials Science and Engineering: A 2015;642:1–6.
17. Ghalandari L, Tajbakhsh P. Mechanical and Corrosion Properties of Graphene Oxide-Copper Nano-composites produced by the accumulative Roll Bonding (ARB) method. Journal of New Materials 2020;11:43–60.
18. Reihanian M, Hadadian FK, Paydar MH. Fabrication of Al–2vol% Al2O3/SiC hybrid composite via accumulative roll bonding (ARB): An investigation of the microstructure and mechanical properties. Materials Science and Engineering: A 2014;607:188–196.
19. Toroghinejad MR, Jamaati R, Nooryan A, et al. The effect of alumina content on the mechanical properties of hybrid composites fabricated by ARB process. Ceramics International 2014;40:10489–10498.
20. Mahdavian MM, Ghalandari L, Reihanian M. Accumulative roll bonding of multilayered Cu/Zn/Al: An evaluation of microstructure and mechanical properties. Materials Science and Engineering A 2013;579:99–107.
21. Naseri M, Hassani A, Tajally M. An alternative method

for manufacturing Al/B4C/SiC hybrid composite strips by cross accumulative roll bonding (CARB) process. Ceramics International 2015;41:13461–13469.
22. Pirlari AJ, Emamy M, Amadeh AA, et al. Elucidating the effect of TiB 2 volume percentage on the mechanical properties and corrosion behavior of Al5083-TiB 2 composites. Journal of Materials Engineering and Performance 2019;28:6912–6920.
23. Humphreys FJ, Matherly M. The microstructures of deformed two-phase alloys. In: Recrystallization and Related Annealing Phenomena. 2nd ed. Amsterdam: Elsevier Ltd; 2004.
24. Reihanian M, Bagherpour E, Paydar MH. On the achievement of uniform particle distribution in metal matrix composites fabricated by accumulative roll bonding. Materials Letters 2013;91:59–62.
25. Hosford WF. Mechanical Behavior of Materials - Second Edition. second edi. 2009.
26. Malmir N, Alizadeh M, Pashangeh S, et al. Structural characteristics and corrosion properties of Cu/Sn–Pb composite produced by accumulative roll bonding process. Archives of Civil and Mechanical Engineering 2024;24.
27. Mahdavian MM, Khodabandeh AR, Jafarian HR, et al. Evaluation of the macro/microstructure of Al/Cu/Sn/Ni multi-layered composite produced by accumulative-roll-bonding (ARB) and post-heat treatment. Journal of Alloys and Compounds 2022;925:166711.
28. Azushima A, Kopp R, Korhonen A, et al. Severe plastic deformation (SPD) processes for metals. CIRP Annals - Manufacturing Technology 2008;57:716–735.
29. Naghizadeh M, Mirzadeh H. Effects of Grain Size on Mechanical Properties and Work-Hardening Behavior of AISI 304 Austenitic Stainless Steel. Steel Research International 2019;90:1–9.
30. Koterazawa Y. Fractography. Zairyo/Journal of the Society of Materials Science, Japan 1974;23:479–489.
31. Liu S, Tayyebi M, Assari AH, et al. Microstructure, Texture and Tensile Properties of Nickel/Titanium Laminated Composites Produced by Cross Accumulative Roll Bonding Process. Metals and Materials International 2023;29:3630–3644.
32. Fattah-alhosseini A, Naseri M, Alemi MHH. Corrosion behavior assessment of finely dispersed and highly uniform Al/B4C/SiC hybrid composite fabricated via accumulative roll bonding process. Journal of Manufacturing Processes 2016;22:120–126.
33. Reihanian M, Mohammad S, Baghal L, et al. A Comparative Corrosion Study of Al/Al2O3-SiC Hybrid Composite Fabricated by Accumulative Roll Bonding (ARB). Journal of Ultrafine Grained and Nanostructured Materials 2016;49:29–35.
34. Sereshki MA, Azad B, Borhani E, et al. Corrosion Behavior of Commercial Aluminum Alloy Processed by ECAP.pdf. Journal of Ultrafine Grained and Nanostructured Materials 2016;49:22–28.
35. Zakaria HM. Microstructural and corrosion behavior of Al/SiC metal matrix composites. Ain Shams Engineering Journal 2014;5:831–838.
36. Majidabad MA, Rezaei AR, Sabour MR, et al. Mechanical properties and pitting corrosion behavior of Al5085 alloy processed via equal channel angular pressing (ECAP). Journal of Ultrafine Grained and Nanostructured Materials 2023:9–14.